Simulation of superelastic SMA helical springs

Reza Mehrabi[*1] and Mohammad Reza Karamooz Ravari[2]

[1]*Department of Mechanical Engineering, Vali-e-Asr University of Rafsanjan, Rafsanjan, 77139-36417, Iran.*
[2]*Department of Mechanical Engineering, Graduate University of Advanced Technology,
Kerman, 76311-33131, Iran*

Abstract. Shape memory alloy (SMA) helical springs have found a large number of different applications in industries including biomedical devices and actuators. According to the application of SMA springs in different actuators, they are usually under tension and torsion loadings. The ability of SMAs in recovering inelastic strains is due to martensitic phase transformation between austenite and martensite phases. Stress or temperature induced martensite transformation induced of SMAs is a remarkable property which makes SMA springs more superior in comparison with traditional springs. The present paper deals with the simulation of SMA helical spring at room temperature. Three-dimensional phenomenological constitutive model is used to describe superelastic behavior of helical spring. This constitutive model is implemented as a user subroutine through ABAQUS STANDARD (UMAT), and the process of the implementation is presented. Numerical results show that the developed constitutive model provides an appropriate approach to captures the general behavior of SMA helical springs.

Keywords: shape memory alloy; helical spring; martensite transformation; constitutive model; finite element method

1. Introduction

Since the discovery of shape memory alloys (SMAs) in 1962 by Buehler and Wang (Buehler *et al*. 1963, Kauffman and Mayo 1997), they have found several applications in mechanical, civil, medical, and transportation systems due to their superior properties such as superelasticity, shape memory effect, bio-compatibility, and corrosion resistance (Machado and Savi 2003, Mohd Jani *et al*. 2014; Auricchio *et al*. 2015, Menna *et al*. 2015, Pecora and Dimino 2015). The inelastic strain recovery by the unloading is superelastic behavior and shape recovery by the heating is shape memory effect (Zhou *et al*. 2012). The fast demand toward the use of shape memory alloys would lead to fabrication and development of new devices. In this regard, SMA springs are fabricated to use in different industries. Dong *et al*. (2008) numerically and experimentally investigated an SMA spring in airfoil actuator. Dumont and Kuhl (2005) used SMA springs to control active endoscopes. They analyze design optimization by finite element method. Also an experimental and numerical study on SMA helical spring was done by Aguiar *et al*. (2010). Since the cost of such devices can be high in comparison with conventional materials, it is necessary to develop suitable modeling

---

∗Corresponding author, Dr., E-mail: r.mehrabi@vru.ac.ir

approaches to predict their behavior before fabrication. In this regard, several constitutive models have been proposed in the literature (Liang and Rogers 1992, Graesser and Cozzarelli 1994, Brocca *et al.* 2002, Panico and Brinson 2007, Popov and Lagoudas 2007, Mehrabi *et al.* 2014a, Mehrabi *et al.* 2014c, Karamooz ravari *et al.* 2015).

Constitutive models are successfully used for studying the behavior of several SMA devices. Reese and Christ (2008) proposed a finite deformation model for SMAs that includes the effect of pseudoelasticity. They used the finite element method to simulate the mechanical response of NiTi stents. Mirzaeifar *et al.* (2011) studied the superelastic behavior of SMA helical springs under uniaxial loading by use of the analytical and numerical methods. They verified the obtained results with experimental data for NiTi helical spring. Saleeb *et al.* (2013) investigated a finite element analysis of helical springs under uniaxial forces. They showed that the change in coil diameter has an important effect on the response of the helical springs. Some other studies have focused on the modeling, simulation, and experimental study of thermo-mechanical behavior of SMA springs (Attanasi *et al.* 2011, de Aguiar *et al.* 2013, Nicholson *et al.* 2014, Savi *et al.* 2015).

Among different groups of constitutive models including micromechanical models, statistical thermodynamics and phenomenological models, the last one is more preferred. This is because, in these models, material parameters are identified by the experimental tests and the kinetic equations are well implemented into the computer code to be used through a finite element program (Mehrabi *et al.* 2014b). In this paper, a three-dimensional constitutive model based on microplane theory is described and verified with experimental results. As the SMA springs used in actuators are in tensile and/or torsional position, they are under tension and/or torsion loading. Therefore, constitutive model is experimentally and numerically investigated under simple tension and pure torsion loading. Then, the proposed model is performed to investigate the superelastic behaviors of an SMA helical spring. Finite element analyses show that proposed model is a suitable approach to utilize in simulation of SMA devices.

2. Phenomenological model

The microplane model, based on Volumetric-Deviatoric split in a thermodynamically-consistent framework on static constraint is utilized at this paper (Mehrabi *et al.* 2014d). In this approach, macroscopic stress tensor is projected on the micro planes. The 1D constitutive law is defined for associated volumetric and deviatoric stress and strain components on any microplane at a material point. Then, a homogenization process is employed to generalize the 1D relation to a 3D macroscopic one. For this purpose, macroscopic stress is projected to volumetric and deviatoric components in each arbitrary microplane, as illustrated in Fig. 1, using Eq. (1).

$$\boldsymbol{\sigma} = \boldsymbol{\sigma}_{\text{Vol}} + \boldsymbol{\sigma}_{\text{Dev}} \tag{1}$$

Volumetric and deviatoric components of stress are defined as

$$\boldsymbol{\sigma}_{\text{Vol}} = \frac{\text{Tr}(\boldsymbol{\sigma})}{3}\mathbf{1} = \mathbf{I}^{\text{vol}}:\boldsymbol{\sigma}, \boldsymbol{\sigma}_{\text{Dev}} = \boldsymbol{\sigma} - \frac{\text{Tr}(\boldsymbol{\sigma})}{3}\mathbf{1} = \mathbf{I}^{\text{dev}}:\boldsymbol{\sigma} \tag{2}$$

in which $\mathbf{1}$, $\mathbf{I}^{\text{vol}}$ and $\mathbf{I}^{\text{dev}}$ are respectively the second-order identity, volumetric and deviatoric projection tensors (forth-order identity tensor) and are defined as follows

$$\mathbf{I}^{\text{vol}} = \frac{3}{2\pi}\int_{\Omega} \mathbf{V} \otimes \mathbf{V} \, d\Omega = \frac{1}{3}\mathbf{1} \otimes \mathbf{1}, \ \mathbf{I}^{\text{dev}} = \frac{3}{2\pi}\int_{\Omega} \mathbf{Dev}^{\text{T}}.\mathbf{Dev} \, d\Omega = \mathbf{I}^{\text{sym}} - \mathbf{I}^{\text{vol}} \tag{3}$$
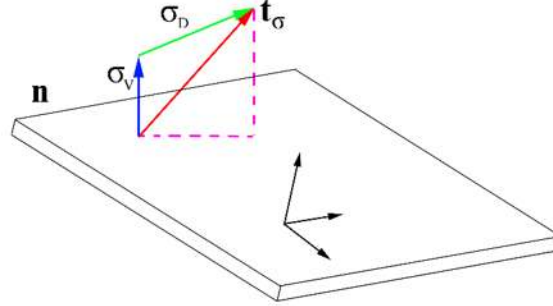
Fig. 1 The Volumetric-Deviatoric (V-D) microplane components of stress

where Ω is the area of a unit hemisphere representing all possible orientations at a material point. Projection tensor $\mathbf{Dev}$ and the transpose of the deviatoric projection tensor $\mathbf{Dev}^{\mathrm{T}}$ are defined as (Leukart and Ramm 2003)

$$\mathbf{Dev} := \boldsymbol{n}.\mathbf{I}^{\mathrm{dev}}, \ \mathbf{Dev}^{\mathrm{T}} := \mathbf{I}^{\mathrm{dev}}.\boldsymbol{n} \tag{4}$$

Stress traction vector on each microplane is shown in Fig. 1, and can be formulated as

$$\boldsymbol{t}_\sigma = \boldsymbol{\sigma}.\boldsymbol{n} = [\boldsymbol{\sigma}_{\mathrm{Vol}} + \boldsymbol{\sigma}_{\mathrm{Dev}}].\boldsymbol{n} = \tfrac{1}{3}[\mathbf{1}:\boldsymbol{\sigma}].\boldsymbol{n} + \boldsymbol{\sigma}_{\mathrm{Dev}}.\boldsymbol{n} = \mathbf{V}:\boldsymbol{\sigma}.\boldsymbol{n} + \boldsymbol{\sigma}_{\mathrm{Dev}}.\boldsymbol{n} = \sigma_{\mathrm{V}}\boldsymbol{n} + \boldsymbol{\sigma}_{\mathrm{D}} \tag{5}$$

It should be noticed that the macroscopic stresses are denoted by $\boldsymbol{\sigma}_{\mathrm{Vol}}$, $\boldsymbol{\sigma}_{\mathrm{Dev}}$ and their counterparts on each microplane are σ_{V} and $\boldsymbol{\sigma}_{\mathrm{D}}$. A standard procedure is used to satisfy the principles of thermodynamic and the necessary constitutive relations are obtained. The microplane volumetric and deviatoric infinitesimal strains based on work conjugate of the microplane stresses are explained as (Mehrabi *et al*. 2014d)

$$\varepsilon_{\mathrm{V}} = -\rho\frac{\partial \mathrm{G}^{\mathrm{mic}}}{\partial \sigma_{\mathrm{V}}}, \boldsymbol{\varepsilon}_{\mathrm{D}} = -\rho\frac{\partial \mathrm{G}^{\mathrm{mic}}}{\partial \boldsymbol{\sigma}_{\mathrm{D}}} \tag{6}$$

The SMA microscopic Gibbs free energy ($\mathrm{G}^{\mathrm{mic}}$) of any plane on the shape memory alloys is

$$\mathrm{G}^{\mathrm{mic}} = \widehat{\mathrm{G}}^{\mathrm{mic}}(\sigma_{\mathrm{V}}, \boldsymbol{\sigma}_{\mathrm{D}}, T, \xi) \tag{7}$$

here the microscopic free energy depends on the stress components $\sigma_{\mathrm{V}}, \boldsymbol{\sigma}_{\mathrm{D}}$ as well as temperature T, and the internal variable ξ. The macroscopic strain tensor is

$$\boldsymbol{\varepsilon} = -\rho\frac{\partial G}{\partial \boldsymbol{\sigma}} = -\rho\frac{3}{2\pi}\int_{\Omega} \frac{\partial G^{\mathrm{mic}}}{\partial \boldsymbol{\sigma}}\, \mathrm{d}\Omega = \frac{3}{2\pi}\int_{\Omega} [-\rho\frac{\partial G^{\mathrm{mic}}}{\partial \sigma_{\mathrm{V}}}\frac{\partial \sigma_V}{\partial \boldsymbol{\sigma}} - \rho\frac{\partial G^{\mathrm{mic}}}{\partial \boldsymbol{\sigma}_{\mathrm{D}}}\frac{\partial \boldsymbol{\sigma}_D}{\partial \boldsymbol{\sigma}}]\, \mathrm{d}\Omega$$
$$= \frac{3}{2\pi}\int_{\Omega} (\varepsilon_{\mathrm{V}}\mathbf{V} + \mathbf{Dev}^{\mathrm{T}}.\boldsymbol{\varepsilon}_{\mathrm{D}})d\Omega \tag{8}$$

The local 1D constitutive equations for the volumetric and deviatoric components are defined as

$$\varepsilon_{\mathrm{V}} = \frac{\sigma_{\mathrm{V}}}{E_{\mathrm{V}}^0}, \boldsymbol{\varepsilon}_{\mathrm{D}} = \frac{\sigma_{\mathrm{D}}}{E_{\mathrm{D}}^0} + \mathbf{R}\varepsilon^*\xi \tag{9}$$

where $\mathbf{R}$ is a vector, ε^* is the uniaxial maximum recoverable strain, and ξ is the martensite

volume fraction determined by Eqs. (10)-(12):

- Conversion to Detwinned Martensite

For $T > T_s^M$ and $\sigma_s^{cr} + C_M(T - T_s^M) < \bar{\sigma} < \sigma_f^{cr} + C_M(T - T_s^M)$

$$\xi = \frac{1-\xi_0}{2}\cos\left\{\frac{\pi}{\sigma_s^{cr}-\sigma_f^{cr}} \times [\bar{\sigma} - \sigma_f^{cr} - C_M(T - T_s^M)]\right\} + \frac{1+\xi_0}{2} \tag{10}$$

For $T < T_s^M$ and $\sigma_s^{cr} < \bar{\sigma} < \sigma_f^{cr}$

$$\xi = \frac{1-\xi_0}{2}\cos\left\{\frac{\pi}{\sigma_s^{cr}-\sigma_f^{cr}} \times [\bar{\sigma} - \sigma_f^{cr}]\right\} + \frac{1+\xi_0}{2} \tag{11}$$

- Conversion to Austenite:

For $T > T_s^A$ and $C_A(T - T_f^A) < \bar{\sigma} < C_A(T - T_s^A)$

$$\xi = \frac{\xi_0}{2}\left\{1 + \cos\left[\frac{\pi}{T_f^A-T_s^A}(T - T_s^A - \frac{\bar{\sigma}}{C_A})\right]\right\} \tag{12}$$

where ξ_0 represents the martensite volume fraction prior to the current transformation, T_f^M, T_s^M, T_s^A, and T_f^A are transformation temperatures, and C_A and C_M are the slopes of austenite and martensite strips in the stress-temperature phase diagram. Also, E_V^0 and E_D^0 are the local linear elastic modulus which can be obtained as a function of the global elastic constants

$$E_V^0 = \frac{E(\xi)}{1-2v}, \ E_D^0 = \frac{E(\xi)}{1+v} \tag{13}$$

where v is Poisson's ratio and E is Young's modulus. Reuss scheme is adopted for the equivalent elastic modulus

$$\frac{1}{E(\xi)} = \frac{1-\xi}{E_A} + \frac{\xi}{E_M} \tag{14}$$

The SMA materials behave as austenite-martensite periodic composites (Auricchio *et al.* 2007). The total elongation of the composite in uniaxial loading is the sum of the elongation of the austenitic and the martensitic parts. It means that austenitic and martensitic parts behave as two springs with different elastic properties acting in series.

Following the standard procedure of the microplane model (Mehrabi *et al.* 2014d), utilizing the homogenization process, the 1D constitutive relation presented in Eq. (1) is generalized to a 3D constitutive one. Accordingly, the macroscopic strain tensor for shape memory alloys is obtained

$$\boldsymbol{\varepsilon} = \boldsymbol{\varepsilon}^e + \boldsymbol{\varepsilon}^{tr} = \frac{3}{2\pi}\int_\Omega \left(\frac{1-2v}{E(\xi)}\mathbf{V}\otimes\mathbf{V}:\boldsymbol{\sigma} + \frac{1+v}{E(\xi)}\mathbf{Dev}^T.\mathbf{Dev}:\boldsymbol{\sigma}\right)d\Omega + \frac{3}{2\pi}\int_\Omega \varepsilon^*\xi\mathbf{Dev}^T.\mathbf{R}\,d\Omega \tag{15}$$

in which vector **R** is defined as

$$R_n = t_n + \frac{1+v}{E(\xi)\varepsilon^*\xi}\sigma_{ij}[-(\frac{1}{2}(\delta_{ni}n_j + \delta_{nj}n_i) - \frac{\delta_{ij}}{3}n_n) + \left(n_in_j - \frac{\delta_{ij}}{3}\right)n_n + \frac{n_it_j + n_jt_i}{2}t_n]$$

$$= t_n + \frac{1+v}{E(\xi)\varepsilon^*\xi}\sigma_{ij}[n_in_jn_n - \frac{1}{2}(\delta_{ni}n_j + \delta_{nj}n_i) + \frac{n_it_j + n_jt_i}{2}t_n]$$

$$\tag{16}$$

An integration technique consisting of 21 Gaussian integration points on the surface of the

hemisphere is utilized to be able to calculate the integral of Eq. (15) (Bažant and Oh 1986).

3. Experimental validation

In this section, proposed constitutive model based on microplane theory is experimentally validated. For this purpose, the numerical results of this approach are compared with recent stress-controlled tension and pure torsion experimental findings for NiTi superelastic torque tubes (Mehrabi *et al*. 2015).

The presented constitutive model is implemented as a user subroutine (UMAT) through the finite element software ABAQUS for numerical investigations. The implemented computational algorithm in UMAT is outlined in Table 1.

Table 1 The numerical algorithm utilized for implementation of the constitutive model

1- Import the strain increment and the stress tensor at the beginning of the increment denoted by $\Delta\boldsymbol{\varepsilon_n}$ and $\boldsymbol{\sigma}_n$.
2- **If** transformation happened, compute: a) Martensite volume fraction: $\xi(\bar{\sigma}, T)$ b) Transformation strain: $\boldsymbol{\varepsilon}^{tr}$ **Else** go to step 3
3- Compute elastic strain: $\boldsymbol{\varepsilon}^e$
4- Compute total strain: $\boldsymbol{\varepsilon} = \boldsymbol{\varepsilon}^e + \boldsymbol{\varepsilon}^{tr}$
5- Compute Jacobian tensor: $$\boldsymbol{C}^{et-1} = \frac{\partial\boldsymbol{\varepsilon}}{\partial\boldsymbol{\sigma}} = \frac{\partial\varepsilon_{ij}}{\partial\sigma_{pq}}$$ $$= \frac{1-2\upsilon}{3E}\delta_{pq}\delta_{ij} + \frac{1+\upsilon}{E}\frac{3}{2\pi}\int_{\Omega}[\frac{1}{2}n_q(\delta_{ip}n_j + \delta_{jp}n_i) - \frac{1}{3}\delta_{ij}n_p n_q]d\Omega$$ $$+ \varepsilon^*\frac{9}{4\pi}\frac{S_{pq}}{\bar{\sigma}}\frac{d\xi_s}{d\bar{\sigma}}\int_{\Omega}(\frac{1}{2}(R_i n_j + R_j n_i) - \frac{\delta_{ij}}{3}n_k R_k)\,d\Omega$$ $$+ \varepsilon^*\xi_s\frac{3}{2\pi}\int_{\Omega}(\frac{1}{2}(\frac{\partial R_i}{\partial\sigma_{pq}}n_j + \frac{\partial R_j}{\partial\sigma_{pq}}n_i) - \frac{\delta_{ij}}{3}n_k\frac{\partial R_k}{\partial\sigma_{pq}})\,d\Omega$$ It should be noted that $S_{pq} = \sigma_{pq} - \frac{\sigma_{mm}}{3}\delta_{pq}$ is deviatoric stress.
6- Compute incremental stress tensor $\Delta\boldsymbol{\sigma} = \boldsymbol{C}^{et}:\Delta\boldsymbol{\varepsilon_n}$
7- Update stress. $\boldsymbol{\sigma}_{n+1} = \boldsymbol{\sigma}_n + \Delta\boldsymbol{\sigma}$
8- End the program

Table 2 Material parameters used in microplane model for experimental verification (Mehrabi *et al*. 2014b)

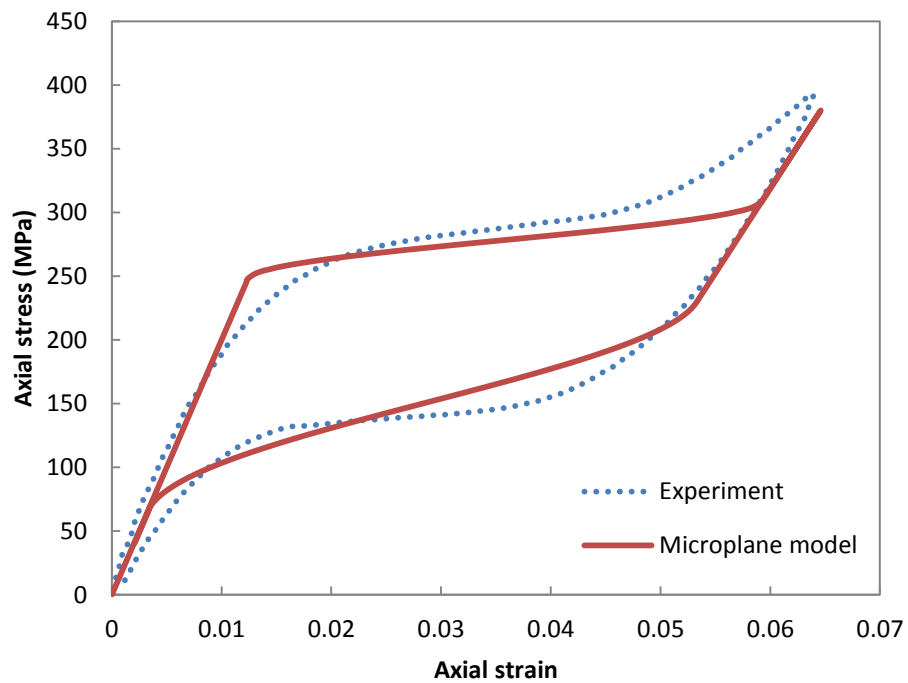| Symbols	Values	Units
E_A	20000	MPa
E_M	13300	MPa
$\upsilon_A = \upsilon_M$	0.33	
T_f^M	-32	°C
T_s^M	-15	°C
T_s^A	-5	°C
T_f^A	15	°C
σ_s^{cr}	20	MPa
σ_f^{cr}	100	MPa
C_M	6	MPa/°C
C_A	8.2	MPa/°C
ε^*	0.038	

Fig. 2 Comparison between the microplane model and experimental results for a thin-walled tube under tension at room temperature
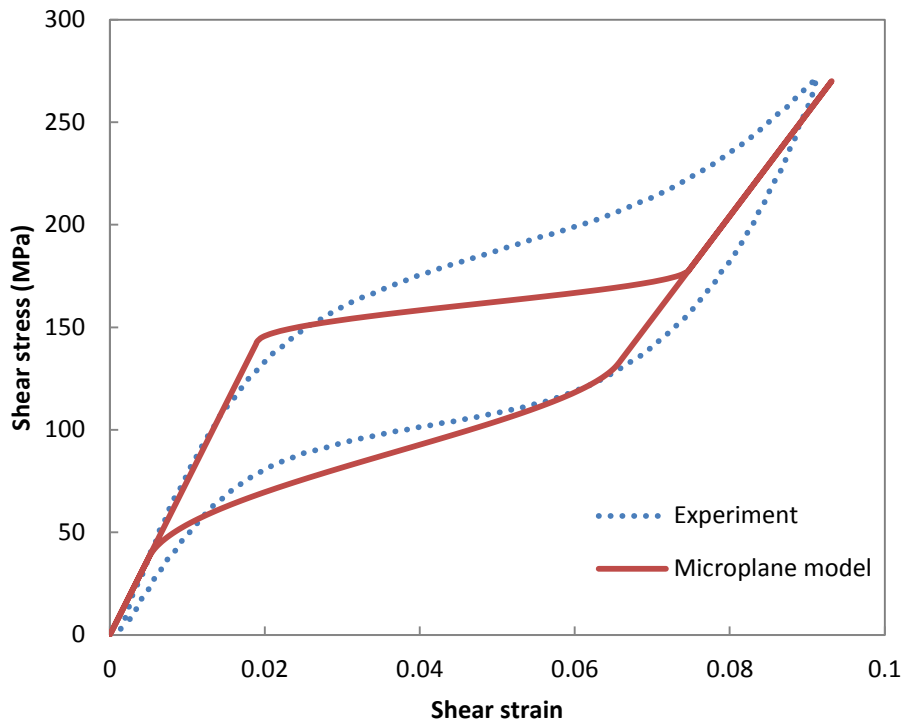
Fig. 3 Comparison between the microplane model and experimental results for a thin-walled tube under pure torsion at room temperature

Simple tension as well as pure torsion test of a torque tube is conducted to investigate the capability of the proposed model in capturing the behavior of SMAs. Material parameters used in the microplane model are calibrated and listed in Table 2. Refer to (Mehrabi and Kadkhodaei 2013) for more details about the calibration of the material parameters based on phase diagram.

Fig. 2 depicts a comparison between the axial stress–strain responses of the microplane model and experimental results. Comparison between microplane model and experimental data in pure torsion are shown in Fig. 3. It is seen that results of microplane model are in good agreement with experimental results in simple tension however, an insignificant discrepancy between simulation and experimental data for the torsion case is found. After showing the capabilities of the microplane model in tensile and torsional loadings, model is used in the simulation of a real SMA device.

4. Numerical results

In this section, the above mentioned constitutive model is used to simulate a SMA device. To do so, a SMA helical spring is modeled in ABAQUS/STANDARD 6.11-1 as shown in Fig. 4. First, a mesh sensitivity study is performed to be assuring about the finite element results similar to what

presented in (Karamooz Ravari and Kadkhodaei 2014, Karamooz Ravari *et al*. 2014). Using this method, the model is meshed using 9453 three dimensional 10-node quadratic tetrahedron elements denoted by C3D10 in ABAQUS. Fig. 4(a) shows an undeformed configuration of SMA helical spring and boundary conditions. This spring has two coils which is simulated with a wire diameter of 4 mm, a spring external diameter of 24 mm, and pitch size of 12 mm. The initial length of spring is 28 mm. As the material parameters used in the proposed model are not mentioned experimentally, here some other common parameters are used. Material parameters that are used for the analysis are extracted from the literatures and are listed in Table 3.

The helical spring is subjected to axial force of 1100 N at one end and is fixed in another end. Comparison of the initial geometry with deformed shape is shown in Fig. 4(b). As shown in this figure, the spring is stretched during the loading step and recovers the initial geometry, as it is expected in the superelastic regime, during the unloading step. Force-displacement response of the loading-unloading on the helical spring is shown in Fig. 5. It is shown that the helical spring shape is fully recovered in unloading step. This result is in qualitative agreement with Arghavani *et al*. (2011) reported in Fig. 6.
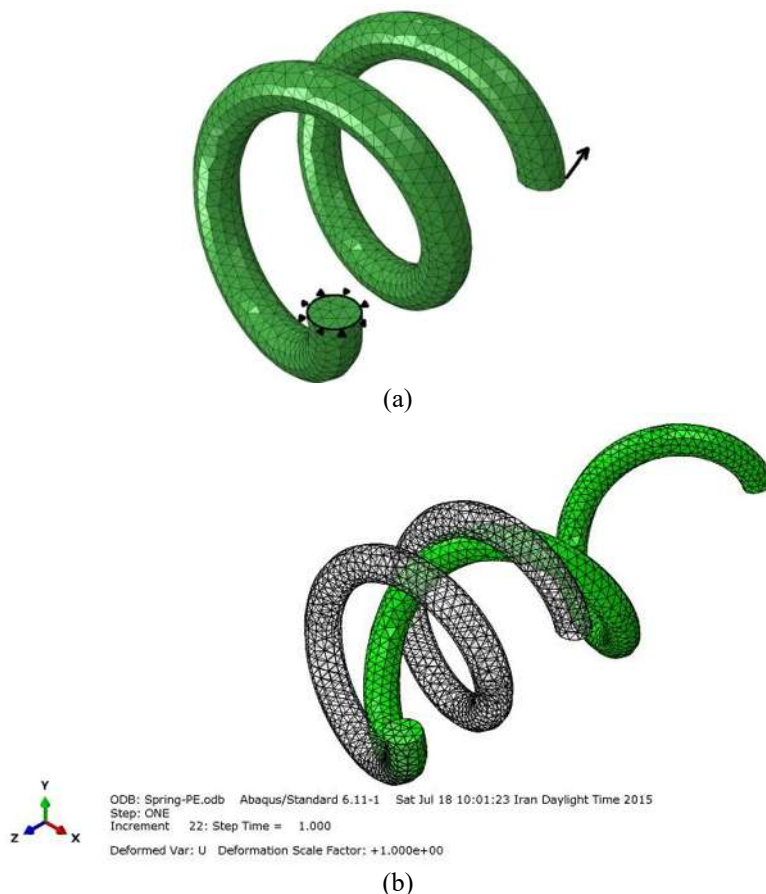

(a)

(b)

Fig. 4 Finite element model for the SMA helical spring (a) Initial geometry and boundary conditions (b) Deformed shape in comparison with undeformed shape
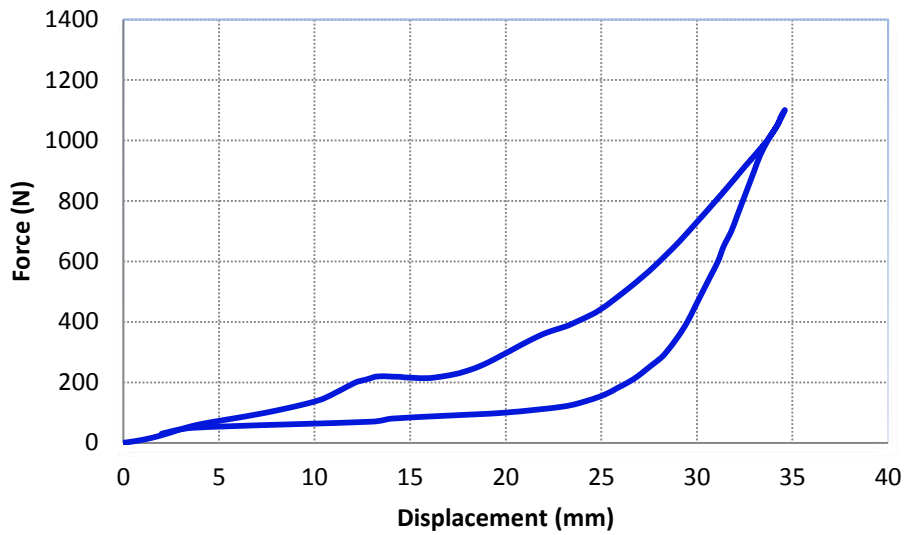
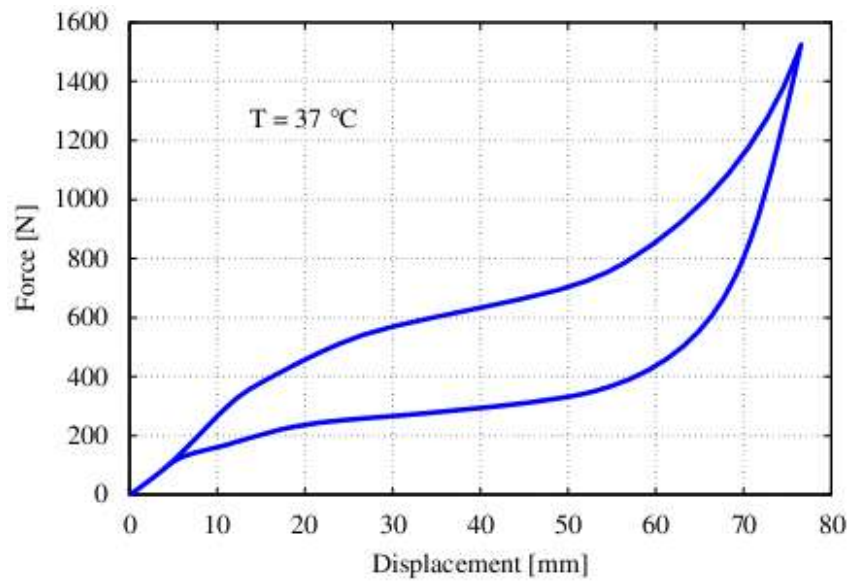Fig. 5 Force-displacement diagram for the superelastic SMA helical spring

Fig. 6 Force-displacement diagram for the SMA spring: pseudo-elasticity (Arghavani *et al*. 2011)

It should be noted that some helical springs are implanted into the patient's body. Therefore, simulation of biomedical devices is an interesting topic and lead to future research.

Table 3 Material parameters used in microplane model for simulation of SMA helical spring

Symbols	Values	Units
E_A	51700	MPa
E_M	51700	MPa
$\upsilon_A = \upsilon_M$	0.33	
T_f^M	-20	°C
T_s^M	-10	°C
T_s^A	0	°C
T_f^A	11	°C
σ_s^{cr}	100	MPa
σ_f^{cr}	185	MPa
C_M	6	MPa/°C
C_A	8.2	MPa/°C
ε^*	0.075	

4. Conclusions

In this paper, the superelastic behavior of SMA helical spring is investigated. For this purpose, a phenomenological constitutive model based on microplane theory is utilized. The proposed model is verified with experimental findings. Good agreement between numerical results and experimental data agitated the authors to use the proposed model for simulation of biomedical devices. A user material subroutine (UMAT) is numerically implemented through the commercial finite element software to simulate the mechanical response of helical spring. Numerical results show that the three-dimensional microplane model provides an appropriate constitutive relation to predict the general behavior of real SMA devices.

References

Aguiar, R.A., Savi, M.A. and Pacheco, Pedro M.C.L. (2010), "Experimental and numerical investigations of shape memory alloy helical springs", S*mart Mater. Struct*., **19**(2), 025008.

Arghavani, J., Auricchio, F., Naghdabadi, R. and Reali, A. (2011), "An improved, fully symmetric, finite-strain phenomenological constitutive model for shape memory alloys", *Finite Elem. Anal. Des*., **47**(2), 166-174.

Attanasi, G., Auricchio, F. and Urbano, M. (2011), "Theoretical and experimental investigation on SMA superelastic springs", *J. Mater. Eng. Perform*., **20**(4-5), 706-711.

Auricchio, F., Boatti, E., *et al.* (2015), Chapter 11 - SMA Biomedical Applications. Shape Memory Alloy Engineering. L. L. Concilio. Boston, Butterworth-Heinemann: 307-341.

Bažant, P. and Oh, B. (1986), "Efficient numerical integration on the surface of a sphere", ZAMM-Journal

of Applied Mathematics and Mechanics/Zeitschrift für Angewandte Mathematik und Mechanik **66**(1): 37-49.

Brocca, M., Brinson, L.C. and Bažant, Z.P. (2002), "Three-dimensional constitutive model for shape memory alloys based on microplane model", *J. Mech. Phys. Solids*, **50**(5), 1051-1077.

Buehler, W.J., Gilfrich, J.V. and Wiley, R.C. (1963), "Effect of low-temperature phase changes on the mechanical properties of alloys near composition TiNi", *J. Appl. Phys.*, **34**(5), 1475-1477.

de Aguiar, R.A.A., de Castro Leão Neto, W.C., Savi, M.A. and Calas Lopes Pacheco, P.M. (2013), "Shape memory alloy helical springs performance: modeling and experimental analysis", Materials Science Forum, 758, 147-156.

Dong, Y., Boming, Z. and Jun, L. (2008), "A changeable aerofoil actuated by shape memory alloy springs", *Mater. Sci. Eng.*, **485**(1), 243-250.

Dumont, G. and Kühl, C. (2005), "Finite element simulation for design optimisation of shape memory alloy spring actuators", *Eng. Comput.*, **22**(7), 835-848.

Graesser, E. and Cozzarelli, F. (1994), "A proposed three-dimensional constitutive model for shape memory alloys", *J. Intel. Mat. Syst. Str.*, **5**(1), 78-89.

Karamooz Ravari, M.R. and Kadkhodaei, M. (2014), "A computationally efficient modeling approach for predicting mechanical behavior of cellular lattice structures", *J. Mater. Eng. Perform.*, 1-8.

Karamooz Ravari, M.R., Kadkhodaei, M., Badrossamay, M. and Rezaei, R. (2014), "Numerical investigation on mechanical properties of cellular lattice structures fabricated by fused deposition modeling", *Int. J. Mech. Sci.*, **88**, 154-161.

Kauffman, G. and Mayo, I. (1997), "The story of nitinol: the serendipitous discovery of the memory metal and its applications", *The Chemical Educator*, **2**(2), 1-21.

Leukart, M. and Ramm, E. (2003), "A comparison of damage models formulated on different material scales", *Comput. Mater. Sci.*, **28**(3), 749-762.

Liang, C. and Rogers, C. (1992), "A multi-dimensional constitutive model for shape memory alloys", *J. Eng. Math.*, **26**(3), 429-443.

Machado, L.G. and Savi, M.A. (2003), "Medical applications of shape memory alloys", *Brazilian J. Medical Bio. Res.*, **36**, 683-691.

Mehrabi, R., Andani, M.T., Elahinia, M. and Kadkhodaei, M. (2014a), "Anisotropic behavior of superelastic NiTi shape memory alloys; an experimental investigation and constitutive modeling", *Mech. Mater.*, **77**, 110-124.

Mehrabi, R. and Kadkhodaei, M. (2013), "3D phenomenological constitutive modeling of shape memory alloys based on microplane theory", *Smart Mater. Struct.*, **22**(2), 025017.

Mehrabi, R., Kadkhodaei, M., Taheri Andani, M. and Elahinia, M. (2014b), "Microplane modeling of shape memory alloy tubes under tension, torsion, and proportional tension–torsion loading", *J. Intel. Mat. Syst. Str.*, 1045389X14522532.

Mehrabi, R., Kadkhodaei, M. and Elahinia, M. (2014c), "Constitutive modeling of tension-torsion coupling and tension-compression asymmetry in NiTi shape memory alloys", *Smart Mater. Struct.*, **23**(7), 75021-75035.

Mehrabi, R., Kadkhodaei, M. and Elahinia, M. (2014d), "A thermodynamically-consistent microplane model for shape memory alloys", *Int. J. Solids Struct.*, **51**(14), 2666-2675.

Mehrabi, R., Taheri Andani, M. Kadkhodaei, M. and Elahinia, M. (2015), "Experimental study of NiTi thin-walled tubes under uniaxial tension, torsion, proportional and non-proportional loadings", *Exp. Mech.*, **55**, 1151-1164.

Menna, C., Auricchio, F., *et al*. (2015), Chapter 13 - Applications of Shape Memory Alloys in Structural Engineering. Shape Memory Alloy Engineering. L. L. Concilio. Boston, Butterworth-Heinemann**:** 369-403.

Mehrabi, R., Taheri Andani, M. Kadkhodaei, M., and Elahinia, M. (2015), "Experimental study of NiTi thin-walled tubes under uniaxial tension, torsion, proportional and non-proportional loadings", *Exp. Mech.*, **55**, 1151-1164.

Mirzaeifar, R., DesRoches, R. and Yavari, A. (2011), "A combined analytical, numerical, and experimental study of shape-memory-alloy helical springs", *Int. J. Solids Struct.*, **48**(3), 611-624.

Mohd Jani, J., Leary, M., Subic, A. and Gibson, M.A. (2014), "A review of shape memory alloy research, applications and opportunities", *Mater. Design*, **56**, 1078-1113.

Nicholson, D.E., Padula II, S.A. and Noebe, R.D., Benafan, O. and Vaidyanathan, R. (2014), "Thermomechanical behavior of NiTiPdPt high temperature shape memory alloy springs", *Smart Mater. Struct.*, **23**(12), 125009.

Panico, M. and Brinson, L. (2007), "A three-dimensional phenomenological model for martensite reorientation in shape memory alloys", *J. Mech. Phys. Solids*, **55**(11), 2491-2511.

Pecora, R. and Dimino, I. (2015), Chapter 10 - SMA for Aeronautics. Shape Memory Alloy Engineering. L. L. Concilio. Boston, Butterworth-Heinemann: 275-304.

Popov, P. and Lagoudas, D.C. (2007), "A 3-D constitutive model for shape memory alloys incorporating pseudoelasticity and detwinning of self-accommodated martensite", *Int. J. Plasticity*, **23**(10), 1679-1720.

Ravari, M.K., Kadkhodaei, M. and Ghaei, A. (2015), "A microplane constitutive model for shape memory alloys considering tension–compression asymmetry", *Smart Mater. Struct.*, **24**(7), 075016.

Reese, S. and Christ, D. (2008), "Finite deformation pseudo-elasticity of shape memory alloys–Constitutive modelling and finite element implementation", *Int. J. Plasticity*, **24**(3), 455-482.

Saleeb, A., Dhakal, B., Hosseini, M.S. and Padula II, S.A. (2013), "Large scale simulation of NiTi helical spring actuators under repeated thermomechanical cycles", *Smart Mater. Struct.*, **22**(9), 094006.

Savi, M.A., Pacheco, P.M.C., Garcia, M.S., Aguiar, R.A., de Souza, L.F.G. and da Hora, R.B. (2015), "Nonlinear geometric influence on the mechanical behavior of shape memory alloy helical springs", *Smart Mater. Struct.*, **24**(3), 035012."

Zhou, L., Zheng, L.J., Zhang, H.R. and Zhang, H. (2012), "Effect of oxygen on microstructure of Ni-43Ti-7Al alloy", *Mater. Res. Innov.*, **16**(2), 115-120.

CC